Korean J. Chem. Eng., 40(10), 2463-2471 (2023)
DOI: 10.1007/s11814-023-1551-7

pISSN: 0256-1115
eISSN: 1975-7220

Investigation on hydrogen storage capacity of spherical activated carbons from ion exchange resins

Tae Gyun Kim*, Dong Won Lee*,, Chang Ha Lee***, Yeon Soo Hong*,†, and Jeong Kwon Suh*,†**

*CO_2 & Energy Research Center, Korea Research Institute of Chemical Technology,
141 Gajeong-ro, Yuseong-gu, Daejeon 34114, Korea
**Department of Advanced Material and Chemical Engineering, University of Science & Technology,
217 Gajeong-ro, Yuseong-gu, Daejeon 34113, Korea
***Department of Chemical and Biomolecular Engineering, Yonsei University,
50 Yonsei-ro, Seodaemun-gu, Seoul 03722, Korea
(*Received 7 March 2023 • Revised 12 July 2023 • Accepted 10 August 2023*)

Abstract−The role of spherical activated carbon from ion exchange resin as an adsorption material for hydrogen storage was researched. Spherical activated carbon samples were prepared from two types of physical activation methods using steam and CO_2. The porosity induced by each method and the resulting hydrogen adsorption performance were compared and evaluated. When the samples had similar BET surface areas, steam activation induced microporous spherical activated carbon to increase hydrogen storage performance at low pressure (~1 bar) under low temperature conditions (under 77 K). CO_2 activation enabled good formation of the 1-2 nm sized pore ratio in the micropores, thus enhancing hydrogen storage performance at high pressure (~200 bar) under ambient temperature (under 298 K). In conclusion, this indicates that there exists a range of spherical activated carbon pore size favorable for hydrogen adsorption, dependent on the pressure range applied.

Keywords: Spherical Activated Carbon, Ion Exchange Resin, Hydrogen Storage, BET Surface Area, Micropore Ratio, 1-2 nm Sized Micropore Ratio

INTRODUCTION

Hydrogen has become an ideal alternative energy source due to concerns of atmospheric pollution and energy depletion from fossil fuels' continued use [1-11]. It is eco-friendly and a sustainable resource as it does not emit pollutants during combustion [7-10, 12-14]. Furthermore, hydrogen is abundantly present and can be more easily obtained than fossil fuels substances such as oil and coal, which need to be excavated from select areas. Therefore, hydrogen fuel has become a major interest as a next generation energy [14]. There are, however, challenges to overcome, whether economical or safety related, for hydrogen fuel to become a norm with the current technology level and infrastructure available [5,6].

Because hydrogen has a low energy density per unit volume, storing it requires compression technology [9,15]. Previously studied hydrogen storage technologies had limitations in implementation in its most practical sense: as a high capacity energy source for transportation [2,5,12,14,16-18]. Traditional hydrogen storage methods such as via cryogenic liquid, hydrogen gas compression, or metal hydrides are not considered attractive [2,3,8,10,12,14,15,18,19]. Storing hydrogen through a cryogenic tank demands a significant amount of energy input due to the need for insulation, which requires a temperature of 20 K. Not to mention, there is also risk of hydrogen loss from evaporation [6,14,15,19,20]. Systems to compress hydrogen require enormous amounts of high pressure in order to realize the demand for high energy storage capacity per volume. Further, safety problems and high costs are incurred due to the large and heavy storage containers that are required to withstand the high pressures [14,15]. Metal hydrides on the other hand have the advantage of being relatively safe compared to the other aforementioned methods, but still require high-temperature conditions to release the stored hydrogen, which can incur high costs and safety concerns [14,15].

The U.S. Department of Energy (DOE) presented more than 6.5 wt.% weight hydrogen storage density as a target for on-board systems [21]. However, previous hydrogen storage methods had difficulties in securing safety and economic efficiency to access DOE targets [2,13,19,21]. Therefore, hydrogen storage research under conditions of safety and economics is required. Among the methods of storage through the on-board system, solid-state hydrogen storage refers to hydrogen storage that uses material as a medium [21]. The technology of storing hydrogen in porous materials through physical adsorption is a representative example [8,9,11,18]. According to the van der Waals principle, hydrogen storage by physical adsorption has the strength of reversibility and fast kinetic, allowing hydrogen molecules to be adsorbed and easily separated [5,8, 10]. In addition, hydrogen storage technology using porous materials can reduce cost and weight when compared to other technol-

†To whom correspondence should be addressed.
E-mail: jshong@krict.re.kr, jksuh@krict.re.kr

ogies. Porous polymers, metal-organic frameworks (MOFs), zeolites and carbon adsorbents such as carbon nanotube (CNT) and activated carbon have been studied as representative porous materials for hydrogen storage [1-10,12-17,19,20,22-32]. Compared with other materials, carbon adsorbents have advantages in metrics of high surface area, weight, reversibility, chemical stability, and thermal stability [9,15,17,18,25]. Activated carbon, which is produced by the carbonization and activation of organic materials, is a frontrunner [9].

Activated carbon is a preferred adsorbent compared to other carbon adsorbents because it has a developed porous structure due to micropore and is easily available at a low cost [12,15]. Activated carbon exists in various forms, such as powder, granule, and spherical [33,34]. Most previous hydrogen storage studies used powdered activated carbon. To use powdered activated carbon in the commercialization process, however, molding process and particle size control processes are essential. A significant decrease in hydrogen adsorption capacity of these powdered activated carbons is inevitable due to these processes. Therefore, the use of spherical activated carbon is advantageous for commercialization since these additional control processes are unnecessary. Moreover, a spherical activated carbon has the advantages of being superior in various properties, which include its abrasion resistance, mechanical strength, smooth surface, liquidity, packing density, micropore volume, and pore distribution [33,34]. These advantages are areas of interest because they can be easily applied to the adsorption process more so than other activated carbon forms [33].

Research is being done around hydrogen storage under low pressure and low temperature (~80 K) environments, as both are favorable conditions for activated carbon adsorption [7,8,18]. However, there are practical limitations because higher pressure and temperature conditions are of the norm in an industrial setting [5,14, 27]. Research has demonstrated that hydrogen storage performance of activated carbon at ordinary temperatures and pressures affects the surface area and the pore size distribution [5,9,28,29]. Therefore, one must be able to control the activated carbon's porosity to reap the benefits of hydrogen adsorption under ambient temperature and higher pressure conditions.

Various materials such as coconut shells, rice husks, biomass, and petroleum pitch have been candidates for the manufacturing of activated carbon [7,9,11,12,15,32,33,35,36]. However, they are all prepared by powdered activated carbon or are modified in spherical forms through later molding processes. Unlike conventional precursors, ion exchange resins can be manufactured from spherical activated carbon without any additional process. Spherical activated carbon prepared by ion exchange resin has excellent strength and packing density with the advantage of maintaining its spherical form during its carbonization and activation process [27,37]. This method also affects porosity by modifying the resin's cross-linking to adjust the pores' structure and volume through activation time [27,37,38]. This activation process can be done by chemical or physical activation methods. Chemical activation is performed through carbon erosion and oxidation reactions by chemicals such as H_3PO_4, Na_2CO_3, NaOH, and KOH [6,7,11]. Physical activation involves burning and vaporizing carbon through gases such as steams and CO_2 [9,36]. Both methods can induce higher surface area and microporosity of activated carbon.

Research is being done to induce differences in porosity by doping metal in activated carbon to improve hydrogen adsorption through the spillover effect [2-4,12-14,17,20,24-26]. However, the doped metal reduces the surface area for physical adsorption in super-activated carbon, diminishing the overall hydrogen adsorption performance as pressure rises [24]. One research used hydrogen adsorption performance by inducing porosity improvements via differences in activation conditions [5-9,18,31]. As part of this research, You et al. tested hydrogen adsorption performance by producing activated carbon with ion exchange resin as precursor [27]. However, the induction of porosity difference in porosity was limited to the steam activation time of resins with different cross-linking%. In this study, physical activation was done with steam and CO_2 to induce enhanced porosity (higher surface area and pore distribution). Activation time was increased to induce different porosity of its samples. Textual properties and shapes of prepared samples were analyzed using scanning electron microscopy (SEM) and measuring N_2 absorption/desorption at 77 K. The hydrogen adsorption experiments were carried out under 77 K with low pressure and 298 K with high pressure, respectively, to investigate performance. The study evaluated the favorable condition of hydrogen adsorption and activating condition by measuring the sample's characteristic and performance of hydrogen storage.

EXPERIMENTAL

1. Preparation of the Activated Carbon Adsorbent

The production methods of activated carbon were carried out in two ways: steam activation and CO_2 activation. In this experiment, spherical resin-based activated carbon was prepared by using ion exchange resin, which was named RAC. The resin used gel-type strong acid cation exchange resin (Dow Chemical, AMBERLITE™ IR 120H) composed of polystyrene, with an 8% divinylbenzene (DVB) content as a cross-linking agent. Results from previous studies indicated that a strong acid cation exchange resin, which has a sulfonic acid as a functional group, can easily form spherical activated carbon because the sulfur can form a sulfonyl bridge [39,40].

Both steam activated carbons and CO_2 activated carbons were prepared by a carbonization and an activation process using a rotary tube furnace after drying resin in the oven at 383 K for 24 hours. The same carbonization process was carried out for both samples by placing the dried sample to the rotating tube and raising the temperature to 1,173 K with 6 K/min under an N_2 atmosphere. The steam activated samples were run through the activation process by maintaining the temperature under a N_2 atmosphere containing 65% steam of the carbonized sample when the temperature reached 1,173 K. The steam injection time was adjusted differently to 0.5, 1, 2, 2.25, 2.5, 3, 4, and 5 hours to induce porous differences in the samples. They were named RAC-H_2O-0.5 and 1, 2, 2.25, 2.5, 3, 4, and 5, respectively. The CO_2 activated carbon samples were produced by performing the activation process: maintaining 1,173 K while continuously injecting CO_2 1 L/min through a quantitative pump. Similar to steam activation, activation time was adjusted to induce distinctions in porosity in samples. During

the activation process, the temperature holding time was adjusted differently to 7, 9, 12, 15, 18, 19 and 23 hours in the CO_2 atmosphere. They were named RAC-CO_2-7, 9, 12, 15, 18, 19 and 23, respectively.

2. Characterization of Activated Carbon

The porosity of activated carbon, such as surface area, pore volume, and pore size distribution, was analyzed through N_2 adsorption/desorption isotherms measured at 77 K using a volumetric adsorption apparatus. The surface area was determined by the Brunauer-Emmet-Teller (BET) formula, and the total pore volume value was measured at a relative pressure of P/P_0=0.99. Pore size distribution, micropore volume, and mesopore volume were analyzed through non-local density functional theory (NLDFT) method. All samples were pretreated at 623 K for more than four hours. The morphological characteristics of the samples were analyzed using scanning electron microscopy (SEM, TM3000 of Hitachi).

3. Hydrogen Uptake Measurements

Measurements of hydrogen storage performance were carried out with hydrogen adsorption up to 1 bar at 77 K and up to 200 bar at 298 K. All adsorption experiments were conducted through volumetric methods by using an adsorption apparatus. Hydrogen uptake at 77 K up to 1 bar was carried out by using a Micromeritics, 3Flex 3500 instrument. Samples were pretreated in a vacuum at 623 K for more than 4 hours before adsorption measurement. Hydrogen uptake at 298 K up to 200 bar was performed with a Quantachrome, iSorb HP1 high pressure sorption apparatus with a thermostatic circulator attached. Prior to the measurement, samples were pretreated in a vacuum at 573 K for 4 hours. The hydrogen used for all measurements was ultra-high purity hydrogen (99.999%) in order to reduce the effect of impurity as much as possible.

RESULTS AND DISCUSSION

1. Characterization of Activated Carbons

Table 1 summarizes the textural properties of the spherical activated carbon samples prepared in this study. Both series of RAC-H_2Os and RAC-CO_2s were produced to be as similar as possible in terms of BET surface area. The CO_2 activation time was maintained longer than the steam-activation. It was judged that the activation time must be maintained for a long time in order to obtain similar BET surface area of the steam activated samples at a temperature of 1,173 K due to weak oxidation of activated carbon by CO_2 and release of volatile substances [41]. Burn-off percentages of RAC-H_2Os were increased from 68% to 99% by elevating activation time from 0.5 to 5 hours. As a result, the BET surface area was enhanced from 1,016 m^2/g to 2,825 m^2/g, and the total pore volume also increased gradually from 0.39 cm^3/g to 1.84 cm^3/g. RAC-CO_2s showed burn-off percentage increased continuously from 70% to 97% as activation time increased from 7 hours to 23 hours. The BET surface area increased from 1,058 m^2/g of RAC-CO_2-7 to 2,222 m^2/g of RAC-CO_2-18. However, RAC-CO_2-19 with more activation time showed a stagnant value of 2,225 m^2/g and RAC-CO_2-23 showed a significant reduction of 1,830 m^2/g. The total pore volume increased continuously from 0.44 cm^3/g of RAC-CO_2-7 to 1.60 cm^3/g of RAC-CO_2-19. However, RAC-CO_2-23 showed a lower value of 1.48 cm^3/g as its BET surface area decreased. Eventually, development of porosity such as enhanced BET surface area and total pore volume of the samples emerged as the steam activation process was continued for longer time. However, the CO_2 activation showed a continuous improvement in the porosity of the samples due to an increase in the activation process time and then decreased again. Advanced porosity of activated carbon

Table 1. Textural properties of activated carbon samples

Sample name	Activation time (h)	Burn-off (%)	S_{BET} (m^2/g)	V_{total} (cm^3/g)	V_{micro} (cm^3/g)	V_{meso} (cm^3/g)	V_{micro}/V_{total} (%)	V_{meso}/V_{total} (%)
RAC	0	57	290	0.13	0.13	0	100	0
RAC-H_2O-0.5	0.5	68	1,016	0.39	0.39	0	100	0
RAC-H_2O-1	1	85	1,309	0.57	0.55	0.02	96	4
RAC-H_2O-2	2	90	1,779	0.85	0.79	0.06	93	7
RAC-H_2O-2.25	2.25	93	2,089	0.97	0.82	0.16	84	16
RAC-H_2O-2.5	2.5	94	2,276	1.11	0.85	0.26	77	23
RAC-H_2O-3	3	97	2,471	1.30	0.86	0.44	66	34
RAC-H_2O-4	4	98	2,686	1.53	0.78	0.75	51	49
RAC-H_2O-5	5	99	2,825	1.84	0.75	1.09	41	59
RAC-CO_2-7	7	70	1,058	0.44	0.42	0.02	95	5
RAC-CO_2-9	9	76	1,307	0.61	0.53	0.08	87	13
RAC-CO_2-12	12	85	1,749	0.97	0.69	0.28	71	29
RAC-CO_2-15	15	90	2,079	1.26	0.74	0.52	59	41
RAC-CO_2-18	18	94	2,222	1.50	0.69	0.81	46	54
RAC-CO_2-19	19	96	2,225	1.60	0.67	0.93	42	58
RAC-CO_2-23	23	97	1,830	1.48	0.56	0.92	38	62

S_{BET}: BET surface area, V_{total}: Total pore volume, V_{micro}: Micropore volume, V_{meso}: Mesopore volume, V_{micro}/V_{total}: Micropore ratio, V_{meso}/V_{total}: Mesopore ratio

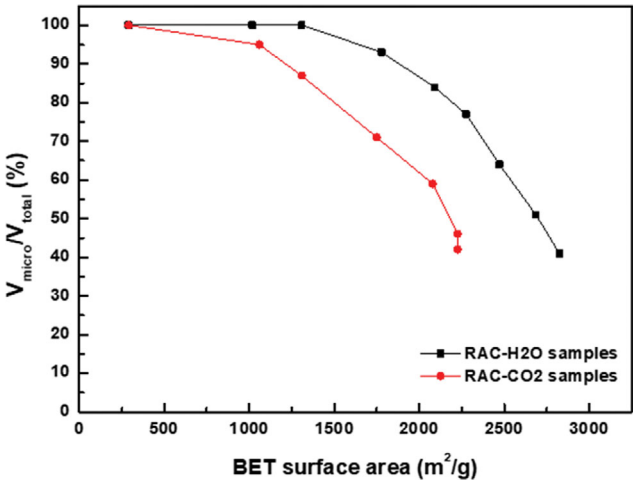

Fig. 1. V_{micro}/V_{total} (%) difference depending on BET surface area (m^2/g).

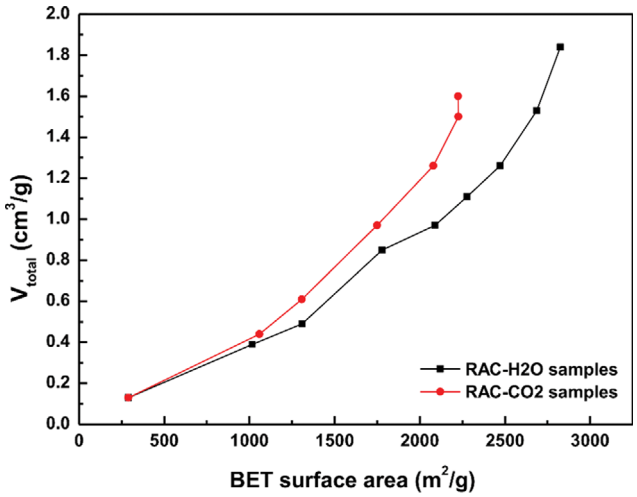

Fig. 2. V_{total} (cm^3/g) difference depending on BET surface area (m^2/g).

can have a significant impact on improving hydrogen storage performance [31,32].

The relationship between the continuously increasing BET surface area and the micropore ratio formed accordingly is shown in Fig. 1. When comparing RAC-H_2Os and RAC-CO_2s with similar BET surface areas, the micropore ratio was higher for steam activated samples. This indicated that the steam activation was more effective in forming activated carbon with high micropore ratio than the CO_2 activation when a similar BET surface area is obtained. However, the total pore volume showed a higher value for RAC-CO_2s.

Fig. 2 compares the difference in total pore volume due to the increase in BET surface area. RAC-CO_2s had higher total pore volume than RAC-H_2Os with similar BET surface area. This indicated that CO_2 activation was superior in increasing the mesopore ratio. Compared with similar BET surface areas, the packing density of RAC-CO_2s was lower than that of RAC-H_2Os. This was due to the higher total volume of RAC-CO_2s.

The type of pores in activated carbon was determined by the

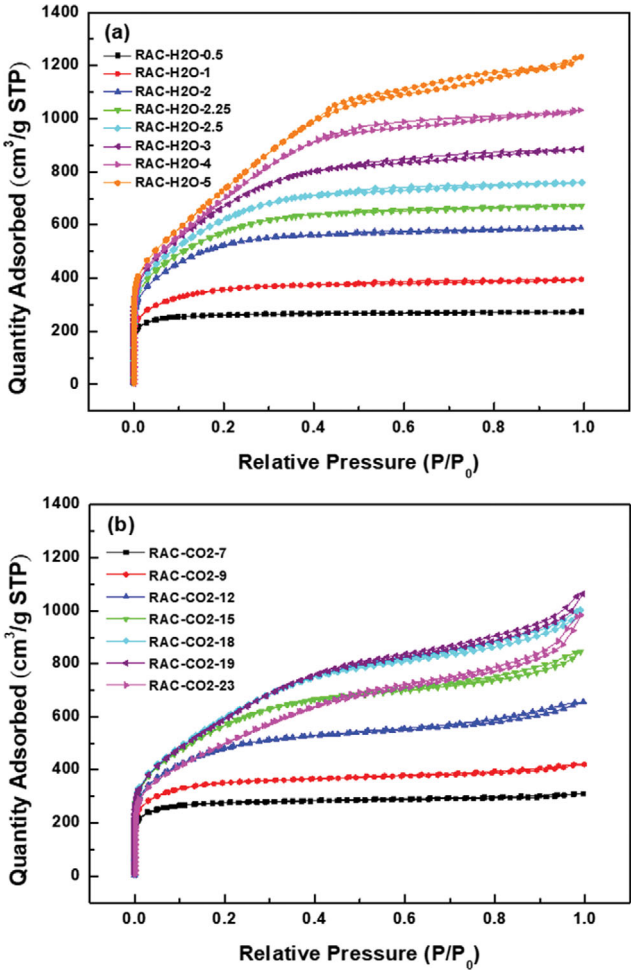

Fig. 3. N_2 adsorption isotherms at 77 K for prepared activated carbons: (a) RAC-H_2O samples, (b) RAC-CO_2 samples.

analysis of N_2 adsorption/desorption isotherms curves. N_2 adsorption/desorption isotherms at 77 K for RAC-H_2Os and RAC-CO_2s are shown in Fig. 3. Adsorption of the low relative pressure area up to 0.1 is caused by existence of micropores [8,15,44,45]. However, the area from relative pressure of 0.1 to saturated pressure indicates the effect of the mesopore, where capillary condensation occurs. Considering the micropore ratios of both RAC-H_2Os and RAC-CO_2s, the isotherms of samples with more than 80% showed Type I form (IUPAC classification) observed in microporous solid. Since then, activation time was further increased, and isotherms of samples with less than 80% micropore ratio observed a hysteresis loop, a characteristic of the sample with mesopore, occurring in the desorption curve at the point of a relative pressure of 0.4 or higher. Thus, Type IV (IUPAC classification) form that the curves of adsorption and desorption do not match each other was shown. Eventually, as activation time increased, isotherms of RAC-H_2Os and RAC-CO_2s changed from Type I to Type IV, and the hysteresis phenomenon became apparent. This phenomenon is known to occur as the size of the micropore expands over a longer activation time, or it would develop into a mesopore by collapse [27,42,43]. Table 1 shows that the micropore ratio of RAC-H_2Os decreased from 100% to 41%, and that of RAC-CO_2s decreased from

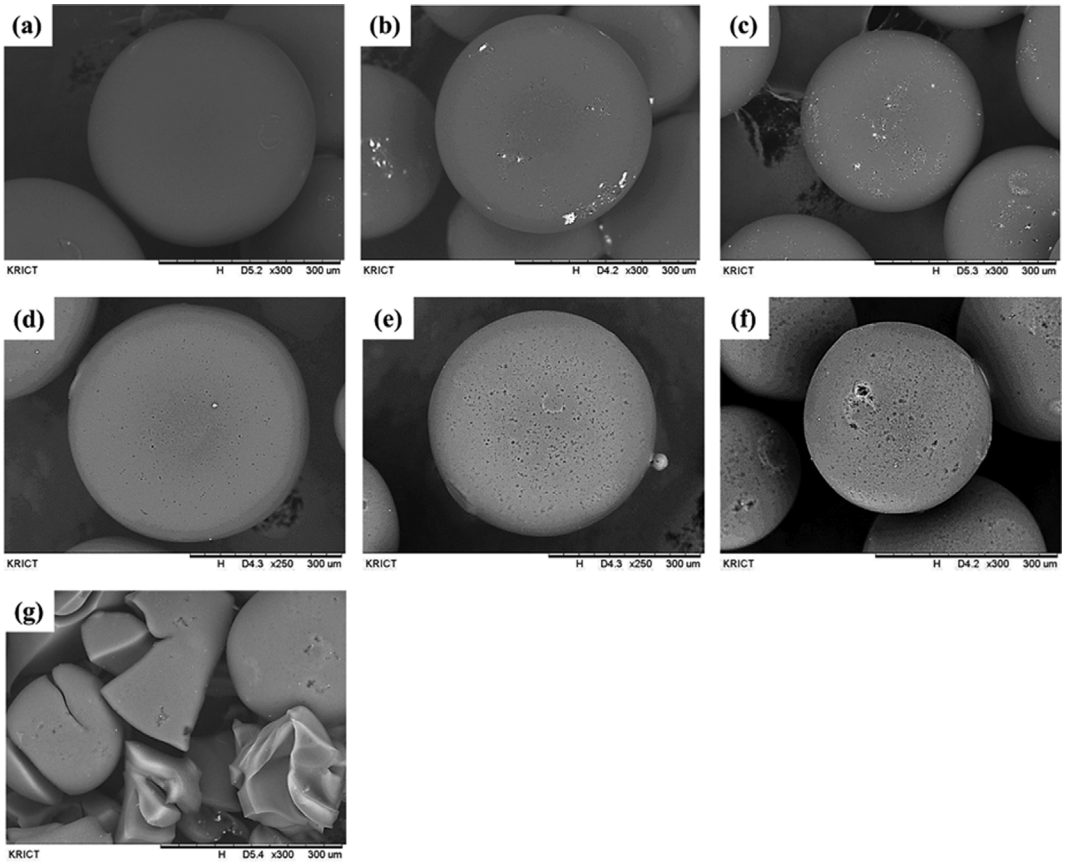

Fig. 4. Scanning electron microscopy (SEM) images of prepared activated carbons: (a) RAC-H_2O-0.5, (b) RAC-H_2O-2, (c) RAC-H_2O-5, (d) RAC-CO_2-7, (e) RAC-CO_2-12, (f) RAC-CO_2-19, (g) RAC-CO_2-23.

95% to 38%, while the mesopore ratio increased from 0% to 59% and 5% to 62% for them, respectively. In conclusion, with the longer the activation process, the porosity phase changed from microporosity to mesoporosity.

Fig. 4 shows the scanning electron microscopy (SEM) images of the change in morphological characteristics due to the activation time of the samples. The RAC-H_2Os images shown in (a)-(c) reveal differences in particle size and surface conservation as the activation time increased from 0.5 to 5 hours. The RAC-H_2O-0.5 with the shortest activation time shows a smooth surface (Fig. 4(a)). Afterwards, in RAC-H_2O-2 and 5 with more activation time, the occurrence of rough surfaces and pores on the surface is observed (Fig. 4(b)-(c)). In particular, the pores and roughness of surface are more prominent on the sample with the longest activation time (i.e., RAC-H_2O-5). Here, the pore on the sample surface is difficult to contribute to the formation of micropore or mesopore, which indicates the loss of large carbon fragments [27]. Likewise, as the activation time of RAC-CO_2s was increased from 7 to 23 hours, the samples' particle sizes became much smaller, and more pores were created on the surface (Fig. 4(d)-(f)). As the pore size increased noticeably due to the loss of the carbon fragment from RAC-CO_2-19, however, RAC-CO_2-23, the sample with the longest activation time, shows a complete collapse (Fig. 4(g)). It was confirmed that the maintenance of spherical activated carbon forms also affected the textural properties shown in Table 1. Both RAC-H_2O and RAC-CO_2 series show continuous porosity improvement in samples that maintain the spherical form despite the prolonged activation process. However, RAC-CO_2-23, which did not maintain a spherical shape, showed a decreased porosity. The effect of porosity due to maintaining the form may contribute to hydrogen adsorption performance.

The International Union of Pure and Applied Chemistry (IUPAC) classifies adsorbent pores as micropore (less than 2 nm), mesopore (between 2 nm and 50 nm) and macropore (greater than 50 nm) according to their size [46]. Pores of activated carbon affect porosity according to its size, and it determines adsorption performance of hydrogen. Therefore, it is necessary to produce a proper pore size in order to utilize the material most effectively for hydrogen storage, and it needs to be figured out. The pore size distribution (PSD) of each sample was investigated to determine the change in the pore size due to the adjustment of the activation time of the prepared activated carbon. The PSDs of RAC-H_2Os and RAC-CO_2s were calculated by non-local density functional theory (NLDFT) and they are shown on Fig. 5. Both series of samples show a noticeable expansion in the range of mesopore with increased activation time. However, many studies have reported that micropore is more advantageous to have superior hydrogen storage performance because pores larger than 2 nm have insufficient energy to store hydrogen [5,6,8]. The distribution of micropore of RAC-H_2Os and RAC-CO_2s shows a noticeable difference in the 1-2 nm sized pore distribu-

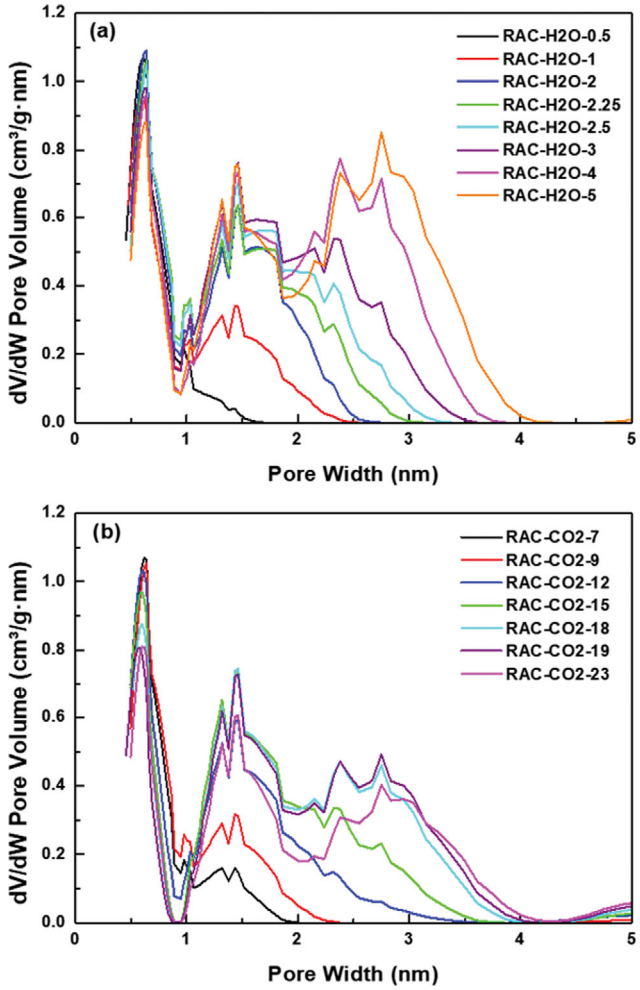

Fig. 5. Pore size distribution of prepared activated carbons: (a) RAC-H_2O samples, (b) RAC-CO_2 samples.

tion of samples with BET surface area of less than 1,700 m^2/g.

This difference can also be seen in Table 2, which shows the pore volume of 0-1 nm and 1-2 nm sized micropores, named as $V_{0\text{-}1\,nm}$ and $V_{1\text{-}2\,nm}$, respectively. The $V_{1\text{-}2\,nm}$ of samples with a BET surface area of less than 1,700 m^2/g is significantly smaller than the $V_{0\text{-}1\,nm}$. Afterwards, samples with BET surface area of more than 1,700 m^2/g show the aspect of $V_{1\text{-}2\,nm}$ being larger than $V_{0\text{-}1\,nm}$. In particular, the 1-2 nm sized micropore ratio ($V_{1\text{-}2\,nm}/V_{micro}$) of RAC-$H_2O$s and RAC-$CO_2$s increase consecutively from 8% to 66% and from 21% to 69% respectively, in proportion to the BET surface area improved with longer activation times. Among the RAC-CO_2s, RAC-CO_2-18, 19 show almost constant in BET surface area, but $V_{1\text{-}2\,nm}/V_{micro}$ was 66% and 69%, respectively, with RAC-CO_2-19 showing higher values. This is much better than $V_{1\text{-}2\,nm}/V_{micro}$ (66%) of RAC-H_2O-5 with higher BET surface area. Afterwards, RAC-CO_2-23 which had decreased porosity shows a lower value of 64% again. From such data, it can be determined that the CO_2 activation has an advantage in enhancing 1-2 nm sized micropore ratio. You et al. reported that this 1-2 nm sized pore, among micropores, can contribute to hydrogen adsorption at high pressure [27].

Table 2. Pore volume of micropores in prepared activated carbons

Sample name	$V_{0\text{-}1\,nm}$ (cm^3/g)	$V_{1\text{-}2\,nm}$ (cm^3/g)	$V_{0\text{-}1\,nm}/V_{micro}$ (%)	$V_{1\text{-}2\,nm}/V_{micro}$ (%)
RAC-H_2O-0.5	0.36	0.03	92	8
RAC-H_2O-1	0.37	0.17	68	32
RAC-H_2O-2	0.36	0.43	46	54
RAC-H_2O-2.25	0.36	0.46	44	56
RAC-H_2O-2.5	0.34	0.51	40	60
RAC-H_2O-3	0.31	0.55	36	64
RAC-H_2O-4	0.28	0.50	35	65
RAC-H_2O-5	0.26	0.49	34	66
RAC-CO_2-7	0.33	0.09	79	21
RAC-CO_2-9	0.34	0.19	64	36
RAC-CO_2-12	0.29	0.40	42	58
RAC-CO_2-15	0.26	0.48	35	65
RAC-CO_2-18	0.23	0.45	34	66
RAC-CO_2-19	0.21	0.46	31	69
RAC-CO_2-23	0.20	0.36	36	64

$V_{0\text{-}1\,nm}$: 0-1 nm sized micropore volume, $V_{1\text{-}2\,nm}$: 1-2 nm sized micropore volume, $V_{0\text{-}1\,nm}/V_{micro}$: 0-1 nm sized micropore ratio, $V_{1\text{-}2\,nm}/V_{micro}$: 1-2 nm sized micropore ratio

Table 3. Hydrogen uptake capacity (wt.%) of prepared activated carbons measured up to 1 bar and 200 bar, respectively

Sample name	H_2 uptake (wt.%) on 1 bar at 77 K	H_2 uptake (wt.%) on 200 bar at 298 K
RAC-H_2O-0.5	1.55	0.52
RAC-H_2O-1	1.69	0.55
RAC-H_2O-2	1.83	0.63
RAC-H_2O-2.25	1.92	0.68
RAC-H_2O-2.5	1.99	0.69
RAC-H_2O-3	2.02	0.76
RAC-H_2O-4	2.12	0.79
RAC-H_2O-5	2.18	0.81
RAC-CO_2-7	1.53	0.53
RAC-CO_2-9	1.63	0.59
RAC-CO_2-12	1.75	0.65
RAC-CO_2-15	1.83	0.72
RAC-CO_2-18	1.87	0.75
RAC-CO_2-19	1.89	0.82
RAC-CO_2-23	1.77	0.71

2. Hydrogen Uptake Behavior Due to Porosity of Activated Carbon

A hydrogen adsorption test of prepared activated carbon was conducted to investigate the association of hydrogen storage performance with the modified pore properties of samples following activation conditions. The test was measured in volumetric method at 1 bar and 200 bar, respectively. The hydrogen uptake capacity (wt.%) up to each maximum pressure is summarized in Table 3.

First, a low pressure (1 bar) hydrogen adsorption was performed at 77 K. As hydrogen has extremely low energy density per unit

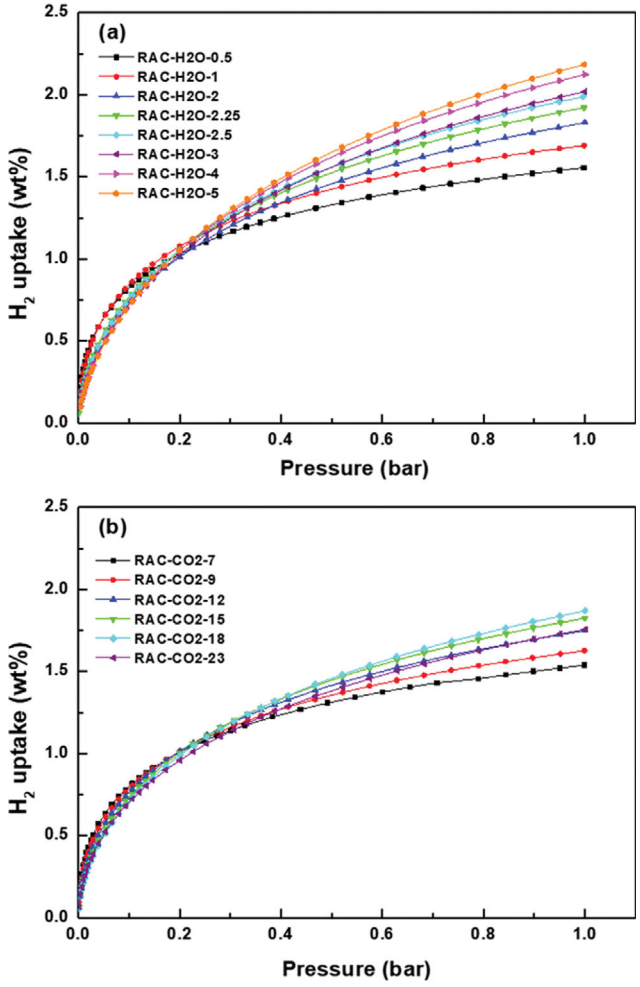

Fig. 6. Hydrogen storage behavior of prepared activated carbons measured up to 1 bar under 77 K, (a) RAC-H_2O samples, (b) RAC-CO_2 samples.

volume, there is a limitation in hydrogen adsorption in ambient temperature where increasing energy density is difficult at low pressure. Therefore, the adsorption proceeded at 77 K, a temperature favorable to physical adsorption. Measured isotherms are shown in Fig. 6. As Table 3 indicates, RAC-H_2Os shows enhanced hydrogen uptake capacity as porosity increased. RAC-CO_2s also showed a continuous increase in hydrogen uptake capacity, but RAC-CO_2-23, which resulted in a decrease in porosity due to the collapse of the spherical form, shows a decreased value. These results are consistent with the results that hydrogen uptake capacity, already known from previous studies, is proportional to porosity such as BET surface area and total pore volume of adsorbent [47-50]. The hydrogen uptake capacity is largely dependent on the textural properties of the carbon materials. High surface area and associated pore volume are clearly responsible for the enhanced hydrogen sorption. The report has shown that it is not just the overall surface area that influences hydrogen uptake in porous carbons, but the surface area associated with 'optimal pores' of a specific size of ca 0.7 nm [49,51]. Thus, surface area associated with 'optimal pores' is also high, which translates to enhanced hydrogen uptake capacity with ambient pressure. But, it can be concluded that pore size larger than the optimal pore size is required under high pressure conditions where multilayer adsorption is likely to occur rather than monolayer adsorption.

RAC-H_2O-5, which has well developed porosity with the highest BET surface area (2,825 m^2/g) of all samples, showed the highest hydrogen uptake capacity at 2.18 wt.%. A previous study reported high hydrogen uptake capacity of up to 2.4 wt.% [7]. Considering that the sample is powdered activated carbon, however, it has a drawback of hydrogen uptake performance reduction due to additional processes such as molding and particle size control for commercialization. In contrast, hydrogen uptake capacity obtained from this study has the advantage of being used in commercial processes without any additional loss due to the property of spherical activated carbon. Between RAC-CO_2s and RAC-H_2Os, which have similar BET surface area, RAC-H_2Os has a higher hydrogen uptake difference from a minimum of 0.02 wt.% to a maximum of 0.12 wt.% (Table 3). As previously identified in Fig. 1, when the same BET surface area was obtained, it was shown to be due to the results that the steam activation could induce a higher micropore ratio than the CO_2 activation. In addition, the result that the 0-1 nm sized micropore ratio ($V_{0\text{-}1\,nm}/V_{micro}$) of RAC-$H_2O$s was higher than that of the RAC-CO_2s with similar BET surface area (Table 2) corresponded with research results that hydrogen adsorption depends on micropore smaller than 1 nm under the same condition [7,8].

Adsorption tests were conducted at 200 bar to measure hydrogen uptake performance at high pressure under ambient temperature, which is a condition applicable to the industry rather than hydrogen storage at extremely low pressure under cryogenic conditions. The experiment was conducted at ambient temperature. The measured isotherms are shown in Fig. 7. Among the RAC-CO_2s and RAC-H_2Os, which had similar BET surface area, RAC-CO_2s had a relatively higher hydrogen uptake capacity difference from a minimum of 0.01 wt.% to a maximum of 0.06 wt.% (Table 3). The RAC-CO_2-19 had the highest final hydrogen uptake capacity of 0.82 wt.%. As expected, the adsorption capacity of RAC-CO_2-23 with porosity degradation decreased. Although the same sample was used, it was much lower than the highest capacity (2.18 wt.%) at low pressure because it was measured under room temperature, which is unfavorable for physical adsorption. The hydrogen uptake capacity at 200 bar of powdered activated carbon measured in the previous study was 1.2 wt.%, better than the results of this study [6]. However, its uptake performance will deteriorate after powder activated carbon experiences the additional process. Thus, the spherical activated carbon used in this study can be seen as a candidate to be applied more favorably from a practical perspective. As with the measurement at low pressure (Fig. 6), the hydrogen uptake capacity at high pressure is also proportional to the porosity of activated carbon. Therefore, it could be confirmed that the relationship between hydrogen adsorption performance and porosity is maintained even if the conditions of temperature and pressure vary. However, when similar BET surface areas were obtained, it was different to the view that hydrogen adsorption would be higher in RAC-H_2Os, a more microporous structure, similar to the results from low-pressure measurements. If so, it may be possible to determine that the more mesoporous structure of the sam-

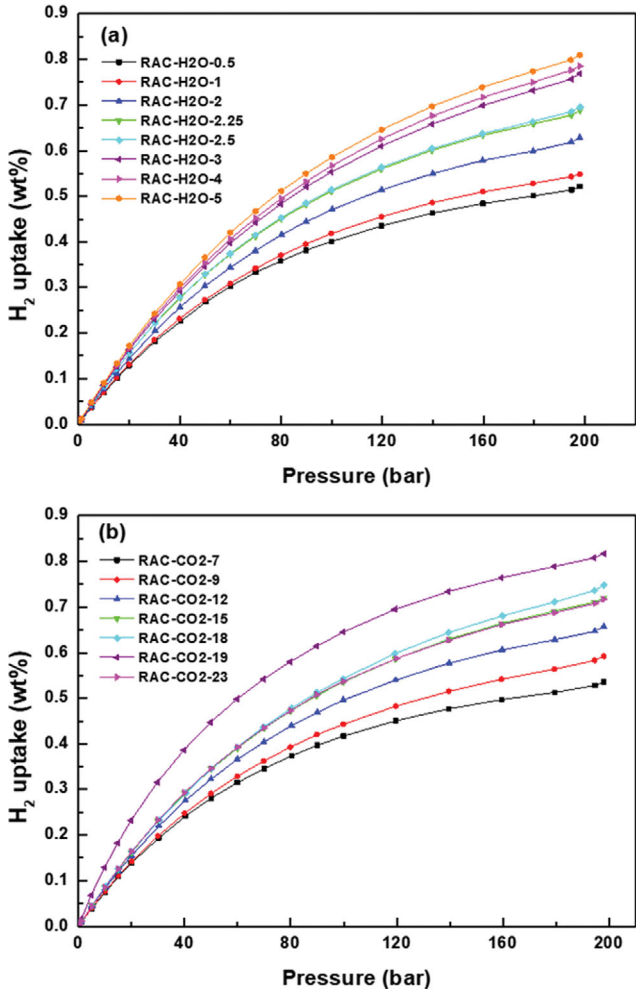

Fig. 7. Hydrogen storage behavior of prepared activated carbons measured up to 200 bar under 298 K, (a) RAC-H_2O samples, (b) RAC-CO_2 samples.

ple has affected hydrogen adsorption. However, since pores over 2 nm have insufficient energy to store hydrogen [5,6,8], mesopore is difficult to affect hydrogen adsorption. In order to figure out why RAC-CO_2s had a superior hydrogen uptake performance at high pressure under ambient temperature, the micropore size distribution was observed in the previous experiment (Fig. 5, Table 2). The CO_2 activation acted in favor of increasing 1-2 nm sized micropore ratio over the steam activation, and it decisively served for hydrogen adsorption at high pressure by enhancing the accessibility of hydrogen to the surface of activated carbon.

CONCLUSIONS

This study compared the modified porosity and the resulting hydrogen adsorption performance of spherical activated carbons prepared by means of physical activation methods using steam and CO_2. Steam activation obtained a continuous improvement in BET surface area in the range of 1,016-2,825 m^2/g in proportion to the activation time. On the other hand, CO_2 activation showed a continuous improvement of 1,058-2,222 m^2/g, but it experienced stagnation of 2,225 m^2/g as the activation time further increased. In the end, the longest activation time sample showed a decreased value of 1,830 m^2/g, revealing a reduced porosity. When the samples had similar BET surface area, the steam activation increased the micropore ratio, and CO_2 activation induced improvement of the mesopore ratio, resulting in higher total pore volume.

The SEM results showed that the changes in surface shape and reduction in particle size as the activation time of each activated carbon increased. However, RAC-CO_2-23 with reduced porosity among CO_2 activated carbon showed a collapse of the spherical form. This failure to maintain the spherical form could be seen to have induced a decrease in porosity.

The pore size distribution, calculated by the NLDFT method, showed that the range of mesopore extended as the activation time increased, over the total pore size range. Both steam activation and CO_2 activation continuously increased the 1-2 nm sized micropore ratio as activation time and BET surface area increased. In particular, the ratio of RAC-CO_2-19 with a BET surface area value of 2,225 m^2/g was 69%, higher than the ratio (66%) of RAC-H_2O-5 with a BET surface area of 2,825 m^2/g. Eventually, it could be seen that CO_2 activation was superior in increasing the 1-2 nm sized pore ratio.

Hydrogen adsorption tests of activated carbon were measured at a low pressure of 1 bar and a high pressure of 200 bar. At 1 bar, steam activated carbons that had more microporous property showed superior hydrogen uptake capacity. The RAC-H_2O-5 showed hydrogen uptake capacity of 2.18 wt.%, the highest value among all the samples. At 200 bar, CO_2 activated carbon revealed superior adsorption performance as a result of increased hydrogen molecule accessibility at high pressure with an improved 1-2 nm sized micropore ratio due to CO_2 activation. RAC-CO_2-19 showed the highest uptake capacity (0.82 wt.%). Each porosity induced by steam activation and CO_2 activation showed a difference in hydrogen adsorption performance under several pressure conditions. Moreover, given that the porosity and hydrogen adsorption of RAC-CO_2-23 where the spherical form collapsed were reduced, it was determined that maintaining the form of spherical activated carbon could also affect hydrogen storage performance.

Conclusively, this study was able to show that spherical activated carbon can be designed to be a possible storage material required for various hydrogen storage conditions, such as low pressure under low temperature and high pressure under ambient temperature. In addition, it can be inferred that the spherical activated carbon would be a more economical and environmentally friendly method to increase hydrogen storage performance without loss, unlike historically used powdered activated carbons. Additionally, the hydrogen storage performance of spherical activated carbon samples prepared in this study is limited in achieving target capacity (6.5 wt.%) of DOE (United States Department of Energy) [21]. However, producing spherical activated carbon using chemical activation at the expense of economic and environmental challenges is expected to increase hydrogen adsorption performance by inducing more porosity.

REFERENCES

1. A. Li, R.-F. Lu, Y. Wang, K.-L. Han and W.-Q. Deng, *Angew. Chem.*,

122(19), 3402 (2010).
2. Y. Li and R. T. Yang, *J. Phys. Chem. C*, **111**(29), 11086 (2007).
3. L. Wang, F. H. Yang, R. T. Yang and M. A. Miller, *Ind. Eng. Chem. Res.*, **48**(6), 2920 (2009).
4. M. Zieliński, R. Wojcieszak, S. Monteverdi, M. Mercy and M. M. Bettahar, *Catal. Commun.*, **6**(12), 777 (2005).
5. K. Xia, J. Hu and J. Jiang, *Appl. Surface Sci.*, **315**, 261 (2014).
6. M. Jordá-Beneyto, F. Suárez-García, D. Lozano-Castelló, D. Cazorla-Amorós and A. Linares-Solano, *Carbon*, **45**(2), 293 (2007).
7. J. Wang, I. Senkovska, S. Kaskel and Q. Liu, *Carbon*, **75**, 372 (2014).
8. K. Xia, Q. Gao, C. Wu, S. Song and M. Ruan, *Carbon*, **45**(10), 1989 (2007).
9. N. Bader and O. Abdelmottaleb, *Environ. Prog. Sust. Energy*, **36**(1), 315 (2017).
10. J. Dong, X. Wang, H. Xu, Q. Zhao and J. Li, *Int. J. Hydrogen Energy*, **32**(18), 4998 (2007).
11. A. Minoda, S. Oshima, H. Iki and E. Akiba, *J. Alloys Compd.*, **580**, S301 (2013).
12. Z. Geng, D. Wang, C. Zhang, X. Zhou, H. Xin, X. Liu and M. Cai, *Int. J. Hydrogen Energy*, **39**(25), 13643 (2014).
13. Y. Li, R. T. Yang, C. J. Liu and Z. Wnag, *Ind. Eng. Chem. Res.*, **46**(24), 8277 (2007).
14. N. Bader and A. Ouederni, *J. Energy Storage*, **13**, 268 (2017).
15. S. S. Samantaray, S. R. Mangisetti and S. Ramaprabhu, *J. Alloys Compd.*, **789**, 800 (2019).
16. P. Chen, X. Wu and K. L. Tan, *Science*, **285**(5424), 91 (1999).
17. I. Rossetti, G. Ramis, A. Gallo and A. D. Michele, *Int. J. Hydrogen Energy*, **40**(24), 7609 (2015).
18. M. Jordá-Beneyto, D. Lozano-Castelló, F. Suárez-García, D. Cazorla-Amorós and A. Linares-Solano, *Micropor. Mesopor. Mater.*, **112**(1-3), 235 (2008).
19. R. Kato and H. Nishide, *Polym. J.*, **50**, 77 (2018).
20. M. Zieliński, R. Wojcieszak, S. Monteverdi, M. Mercy and M. M. Bettahar, *Int. J. Hydrogen Energy*, **32**(8), 1024 (2007).
21. J. Lyu, V. Kudiiarov and A. Lider, *Nanomaterials*, **10**(2), 255 (2020).
22. S. Łoś, M. Letellier, P. Azaïs and L. Duclaux, *J. Phys. Chem. Solids*, **67**(5-6), 1182 (2006).
23. H. Zhou, L. Zhang, S. Gao, H. Liu, L. Xu, X. Wang and M. Yan, *Int. J. Hydrogen Energy*, **42**(36), 23010 (2017).
24. N. P. Stadie, J. J. Purewal, C. C. Ahn and B. Fultz, *Langmuir*, **26**(19), 15481 (2010).
25. K. Chen, Y. Pan and C. Liu, *Sci. China Chem.*, **53**(7), 1598 (2010).
26. Q. Wang, X. Liang, W. Qiao, C. Liu, X. Liu, L. Zhan and L. Ling, *Fuel Process. Technol.*, **90**(3), 381 (2009).
27. Y. W. You, E. H. Moon, I. Heo, H. Park, J. S. Hong and J. K Suh, *J. Ind. Eng. Chem.*, **45**, 164 (2017).
28. B. Panella, M. Hirscher, H. Pütter and U. Müller, *Adv. Funct. Mater.*, **16**(4), 520 (2006).
29. N. L. Rosi, J. Eckert, M. Eddaoudi, D. T. Vodak, J. Kim, M. O'Keeffe and O. M. Yaghi, *Science*, **300**(5622), 1127 (2003).
30. H. W. Langmi, D. Book, A. Walton, S. R. Johnson, M. M. Al-Mamouri, J. D. Speight, P. P. Edward, I. R. Harris and P. A. Anderson, *J. Alloys Compd.*, **404**, 637 (2005).
31. T. P. McNicholas, A. Wang, K. O'Neill, R. J. Anderson, N. P. Stadie, A. Kleinhammes, P. Parilla, L. Simpson, C. C. Ahn, Y. Wnag, Y. Wu and J. Liu, *J. Phys. Chem. C*, **114**(32), 13902 (2010).
32. A. Minoda, S. Oshima, H. Iki and E. Akiba, *J. Alloys Compd.*, **606**, 112 (2014).
33. A. J. Romero-Anaya, M. A. Lillo-Ródenas and A. Linares-Solano, *Carbon*, **48**(9), 2625 (2010).
34. A. J. Romero-Anaya, M. Ouzzine, M. A. Lillo-Rodenas and A. Linares-Solano, *Carbon*, **68**, 296 (2014).
35. Z. Hu and M. P. Srinivasan, *Micropor. Mesopor. Mater.*, **27**(1), 11 (1999).
36. A. S. Ello, L. K. C. de Souza, A. Trokourey and M. Jaroniec, *Micropor. Mesopor. Mater.*, **180**, 280 (2013).
37. D. Malik, A. W. Trochimczuk, A. Jyo and W. Tylus, *Carbon*, **46**(2), 310 (2008).
38. G. Lee, T. Yoon and Z. Shon, *Clean Technol.*, **19**(3), 279 (2013).
39. U. K. Chun, *Proceedings of the 1st workshop on radioactive waste treatment technologies*, Taejon (Korea, Republic of), 28 Oct. 1997, PB286P (1997).
40. M. Matsuda and K. Funabashi, *J. Polym. Sci. Part A: Polym. Chem.*, **25**(2), 669 (1987).
41. S. Guo, J. Peng, W. Li, J, Yang, L, Zhang, S. Zhang and H. Xia, *Appl. Surf. Sci.*, **255**(20), 8443 (2009).
42. W. Xing, S. P. Zhuo and X, Gao, *Mater. Lett.*, **63**(15), 1311 (2009).
43. W. Xing, C. C. Huang, S. P. Zhuo, X. Yuan, G. O. Wang, D. Hulicova-Jurcakova, Z. F. Yan and G. Q. Lu, *Carbon*, **47**(7), 1715 (2009).
44. T. Roussel, R. J. M. Pellenq, M. Bienfait, C, Vix-Guterl, R. Gadiou, F. Beguin and M. Johnson, *Langmuir*, **22**(10), 4614 (2006).
45. R. Gadiou, S. E. Saadallah, T. Piquero, P. David, J. Parmentier and C. Vix-Guterl, *Micropor. Mesopor. Mater.*, **79**(1-3), 121 (2005).
46. K. K. Murray, R. K. Boyd, M. N. Eberlin, G. J. Langley, L. Li and Y. Naito, *Pure Appl. Chem.*, **85**(7), 1515 (2013).
47. Z. Yang, Y. Xia and R. Mokaya, *J. Am. Chem. Soc.*, **129**(6), 1673 (2007).
48. Y. Gogotsi, C. Portet, S. Osswald, J. M. Simmons, T. Yildirim, G. Laudisio and J. E. Fischer, *Int. J. Hydrogen Energy*, **34**(15), 6314 (2009).
49. N. M. Musyoka, M. Wdowin, K. M. Rambau, W. Franus, R. Panek, J. Madej and D. Czarna-Juszkiewicz, *Renew. Energy*, **155**, 1264 (2020).
50. K. C. Kemp, S. B. Baek, W. G. Lee, M. Meyyappan and K. S. Kim, *Nanotechnology*, **26**(38), 385602 (2015).
51. G. Yushin, R. Dash, J. Jagiello, J. E. Fisher and Y. Gogotsi, *Adv. Funct. Mater.*, **16**, 2288 (2006).